Geophysical Research Letters

RESEARCH LETTER
10.1029/2019GL082500

Investigating Subsurface Pathways of Fukushima Cesium in the Northwest Pacific

Ella R. Cedarholm[1], Irina I. Rypina[2], Alison M. Macdonald[2], and Sachiko Yoshida[2]

[1]Earth Science Department, University of New Hampshire, Durham, NH, USA, [2]Woods Hole Oceanographic Institution, Woods Hole, MA, USA

Key Points:
- Kuroshio Extension acts as a permeable barrier to cross-frontal transport of northern waters at the depth of 26.5σ_θ west of ~160°E
- The most likely source of 2013 cesium observed at depth, south of Kuroshio Extension (166°E, 30°N), lies just offshore of Fukushima
- Had deeper samples been obtained at 30°N in 2013, Fukushima-derived cesium might have been observed as deep as ~700 m (26.8σ_θ)

Supporting Information:
- Supporting Information S1
- Movie S1

Correspondence to:
E. R. Cedarholm,
ellacedarholm@gmail.com

Citation:
Cedarholm, E. R., Rypina, I. I., Macdonald, A. M., & Yoshida, S. (2019). Investigating subsurface pathways of Fukushima cesium in the northwest Pacific. *Geophysical Research Letters*, *46*, 6821–6829. https://doi.org/10.1029/2019GL082500

Received 19 FEB 2019
Accepted 7 JUN 2019
Accepted article online 18 JUN 2019
Published online 28 JUN 2019

Abstract Advective pathways for Fukushima Daiichi Nuclear Power Plant (FDNPP)-derived cesium observed in 2013 at 166°E south of the Kuroshio Extension (KE) at >500 m on the 26.5σ_θ isopycnal are investigated. Attention is paid to the KE's role in shaping these pathways. Using a high-resolution model, particle trajectories were simulated backward and forward in time on 26.5σ_θ between the 2013 observations and the 2011 source. A large fraction of backtracked trajectories interacted with the mixed layer just offshore of the FDNPP. The likeliest pathway reaching the deepest 2013 observed cesium location runs along the KE out to ~165°E, where it turns sharply southward. Forward trajectory statistics suggest that for 26.5σ_θ waters originating north of the KE, this current acted as a permeable barrier west of 155–160°E. The deepest 2011 model mixed layers suggest that FDNPP-derived radionuclides may have been present at 30°N in 2013 at greater depths and densities (700 m; 26.8σ_θ).

Plain Language Summary After the 2011 earthquake and ensuing tsunami, radioactive contaminants from Japan's Fukushima Daiichi Nuclear Power Plant entered the ocean just north of the fast-flowing Kuroshio Extension Current. Previous research suggests that strong currents like the Kuroshio and its eastward extension act as barriers, separating the waters to either side. However, the depth to which the barrier effect extends is debated. The accidental discharge of radioactive contaminants provided an opportunity to investigate the vertical extent of the barrier effect. Two years after the accidental discharge, power plant radioactivity was found at depths of half a kilometer on the southern side of the Kuroshio Extension indicating that it must have crossed the frontal barrier (i.e., the current). But where? Using ocean current estimates from a numerical model, thousands of possible pathways that the contamination could have taken were investigated. We found that the radioactive waters probably traveled below the ocean surface along and to the north of the current and were likely unable to cross for thousands of kilometers (about one third of the way across the Pacific). This result suggests that even well below the surface, this current still behaves as a barrier.

1. Introduction

On 11 March 2011 an earthquake and ensuing tsunami hit Japan, which cut power to the Fukushima Daiichi Nuclear Power Plant (FDNPP), causing contaminants from the power plant to enter the ocean via the atmosphere and through leakage of seawater used to cool the reactors. The maximum atmospheric deposition and maximum direct oceanic discharge occurred on 15 March 2011 and 6 April 2011, respectively (Buesseler et al., 2012). Although a tragic event, it has provided an opportunity to improve our understanding of the fate of western Pacific mode waters. In the late spring of 2013, ^{134}Cs, an ocean tracer unique to the FDNPP event, and ^{137}Cs elevated over background levels (Buesseler et al., 2017 and references therein) were observed as deep as 535 m and in waters as dense as 26.5σ_θ at 30°N, at and to the east of 166°E in the western Pacific Basin (Yoshida et al., 2015).

Between the observed location of the FDNPP-derived cesium (henceforth Cs_F) and the power plant, the Kuroshio, the western boundary current that flows along the southern coast of Japan, turns offshore. Warm waters from the south transported by the Kuroshio meet colder northern origin waters transported by the Oyashio, as it separates from the coast, and flows eastward as the Kuroshio Extension (KE) separating the western subarctic gyre from the subtropical gyre (Figure 1). The confluence of these two currents creates a dynamic mixing zone in the region between the KE and Oyashio fronts—appropriately called the mixed water region (MWR, Talley et al., 1995). Here, in the late winter and early spring, radiative forcing, evaporation, and wind cause mixed layers to deepen, creating mode waters, thick homogeneous layers up to several

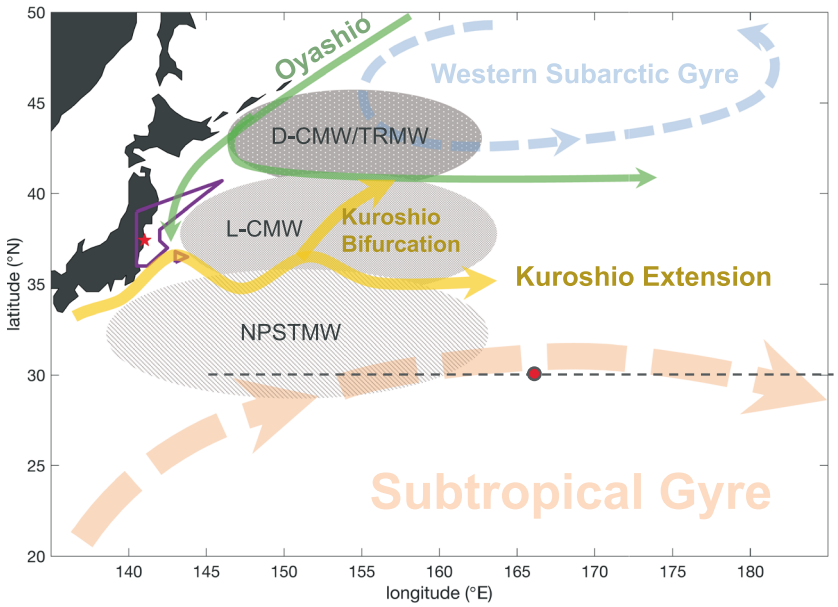

Figure 1. Schematic of surface currents, gyres, and regions of mode water formation: North Pacific Subtropical Mode Water (NPSTMW), Light-Central Mode Water (L-CMW), and Dense-Central Mode Water (D-CMW)/Transition Region Mode Water (TRMW) in the northwest Pacific. Approximate P02 2013 30°N cruise track (dashed line). Red star indicates location of the FDNPP. Purple polygon represents the region of maximum atmospheric deposition, and red circle indicates location of the deepest Cs_F observation (30°N 166.06°E). FDNPP = Fukushima Daiichi Nuclear Power Plant.

hundred meters deep, which are later capped and subducted into the ocean interior. The KE splits (Kuroshio Bifurcation Front) where it encounters the Shatsky Rise (Mizuno & White, 1983; Figure 1) with paths heading both east and northeast. The various frontal zones allow for several different mode water masses to form (Figure 1). North Pacific Subtropical Mode Water (NPSTMW; 24.5–25.9σ_θ) forms to the south of Kuroshio, Light-Central Mode Water (L-CMW; 25.5-26.3σ_θ) forms between the subtropical and subarctic fronts, while Dense-Central Mode Water (D-CMW; 25.9-26.9σ_θ; Bingham & Suga, 2006 and references therein) and Transition Region Mode Water (TRMW; 26.3–26.6σ_θ) form to the north of the subarctic front (Saito et al., 2011). It was into the MWR at the seasonal height of the formation period that FDNPP contamination entered the ocean.

In 2012, subsurface Cs_F was observed to the southwest of the KE in NPSTMW and L-CMW layers (Aoyama et al., 2016; Kumamoto et al., 2014, 2017). These studies surmised that this signal came from atmospheric deposition to the south of the KE, which had been subducted during water mass formation and drawn into the recirculation region. The 2013 30°N zonal transect also measured Cs_F in these water masses (Yoshida et al., 2015). A 2014 165°E survey found Cs_F down to 600 m and concluded that the NPSTMW-subducted signal had spread throughout the subtropics to the west of this latitude within 3 years (Kumamoto et al., 2017).

Between the subtropical and western subarctic gyres, the KE is known to act as a barrier to cross-frontal transport, at least in the surface waters (e.g., Buesseler et al., 2011; Rypina et al., 2013; Rypina, Jayne, et al., 2014**)**. Whether jets act as barriers to cross-stream mixing at depth has been questioned for more than 30 years (Bower et al., 1985). Burkholder and Lozier (2011, 2014) and Garraffo et al. (2014) showed that although jets may act as barriers at the surface, cross-stream transport is stronger at depth and along isopycnals. However, transport across the KE at depth is not fully understood and is the subject of ongoing research. The focus of this study is to (1) use particle trajectory simulations to confirm that the deepest subsurface cesium observed south of the KE in 2013 entered the ocean near FDNPP in 2011, (2) investigate possible pathways between the FDNPP and the location of this deepest cesium, (3) resolve whether this signal could have traveled to the observed location via along-isopycnal advection without diapycnal mixing outside of the MWR, and (4) explore

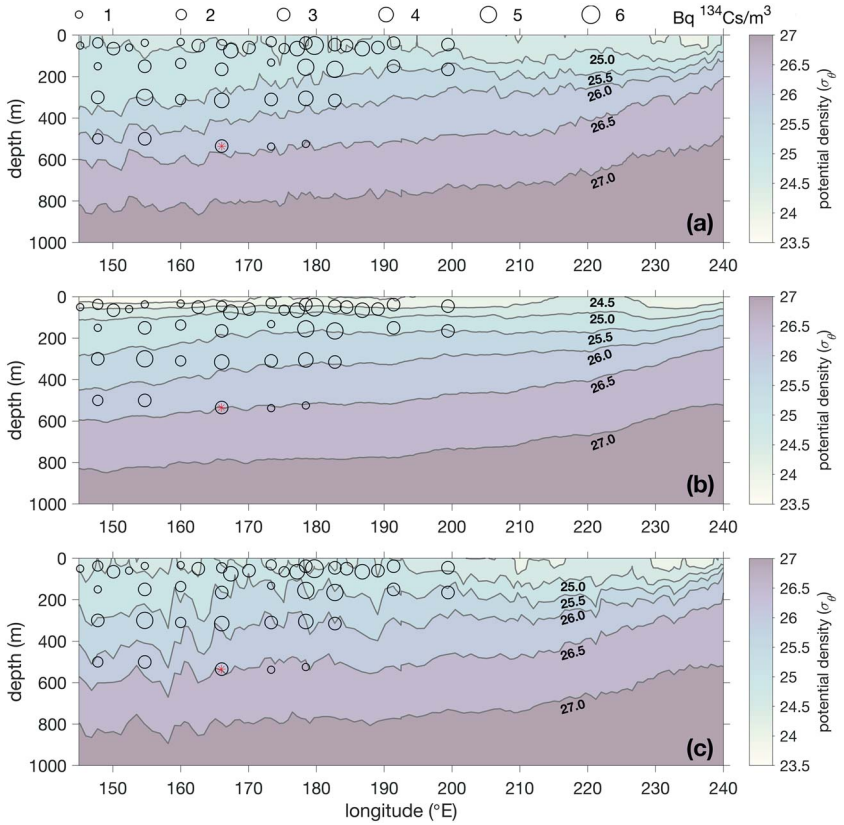

Figure 2. Vertical sections of potential density at 30°N from the surface to 1,000 m with observed ^{134}Cs overlaid as circles with size representing magnitude (units Bq m^{-3}), isopycnals labeled in bold text, and red asterisk highlights the deepest detectable ^{134}Cs. (a) Observed P02 CTD temperature and bottle sample calibrated CTD salinity based densities, (b) 1/12° global HYCOM 2012 mean densities, and (c) HYCOM densities sampled at the time and location of the P02 casts. HYCOM = Hybrid Coordinate Ocean Model.

the spread of the radionuclide-carrying water along the targeted subsurface isopycnal (26.5 σ_θ) and the role of KE as a transport barrier.

2. Data

Daily temperature, salinity, and velocity fields from the date of the maximum atmospheric deposition to the date of the deepest 2013 cesium observation covering the region 135 to 185°E, 20 to 50°N were extracted from global data-assimilating Hybrid Coordinate Ocean Model (HYCOM) GLBa0.08 expt_90.0v output (available at https://www.hycom.org/; Bleck, 2002; Halliwell, 1998). HYCOM has 1/12° horizontal resolution and 33 vertical layers. Further references describing HYCOM are available at the aforementioned link, for example, Cummings and Smedstad (2013). Potential densities were calculated from model temperature and salinity fields using the International Equation of State of Seawater, 1980 formulation (Millero & Poisson, 1981).

In April and May of 2013, a Climate and Ocean: Variability, Predictability and Change (CLIVAR) cruise (P02) transecting the Pacific at 30°N (Figure 1), south of the KE and the MWR, measured ^{134}Cs cesium in water samples. Detectable values were found in many of the collected samples (Figure 2a); the deepest, at the 26.5σ_θ isopycnal, is the focus of this research.

For model output validation, conductivity, temperature, depth (CTD) data from CLIVAR P10 and P02, in situ Argo profiles (http://www.argodatamgt.org; Argo, 2000), and the ISAS-15 0.5° gridded Argo-data-alone product (https://www.seanoe.org, Gaillard et al., 2016; Kolodziejczyk et al., 2017) were used to examine the depth and shape of the density field. Northwest Pacific delayed-time *allsat* Archiving, Validation and Interpretation of Satellite Oceanographic data (AVISO) satellite based 0.25° gridded estimates of surface velocity (http://marine.copernicus.eu) was obtained for the 2011–2013 period. Although considered, the

Gray and Riser (2014) gridded 1° Argo-based velocity fields were not used as they are not presently available for the period of interest.

3. Materials and Methods

3.1. HYCOM Validation

At present, a high-resolution data-assimilating numerical model of the ocean state, such as HYCOM, is arguably the best estimate of subsurface velocity fields on basin scales. However, before proceeding with the particle tracking simulation using HYCOM velocities, we first assessed the numerical model's ability to realistically represent observations in the region of interest. Comparing potential densities derived from the 30°N zonal line (Figure 2a) and 145°E meridional line (Figure S1a in the supporting information) suggests good correspondence in terms of the depth and slope of the subsurface isopycnals to both a HYCOM annual mean (Figures 2b and S1b) and to *synoptic* sections derived from HYCOM sampled at the time and location of the observations (Figures 2c and S1c). The HYCOM annual mean surface waters are lighter than the observations as the latter represent colder late winter and early spring conditions. Along the zonal line at 145°E, the synoptic sampling (Figure 2c) finds a relatively broad meridional gradient in the frontal region, but this feature is likely localized in time as in the annual mean the modeled gradient is more similar to the observed. In the west, in the recirculation region where NPSTMW is formed (Figure 1), the synoptic model section (Figure 2c) suggests stronger local vertical isopycnal displacements than the observations, perhaps due to a mismatch in the timing of local water mass formation events in the model and observations. However, even at fairly small scales, the patterns in the density field suggested by the synoptic section match those observed. To examine the full region of interest, we compared the depth of the $26.5\sigma_\theta$ isopycnal in HYCOM to that observed by profiling floats and compared the HYCOM surface velocity field to satellite altimetry (Text S1 and Figure S2). We concluded from these comparisons that although some seasonality in differences exists, HYCOM reproduces the available observed potential density and velocity fields reasonably well.

3.2. Trajectory Calculations

Assuming no diapycnal mixing, that is, that water parcels move along isopycnal surfaces, it is possible to track their paths in two dimensions using horizontal velocities along a targeted isopycnal. Here, these along-isopycnal velocities were interpolated from HYCOM's discrete depth output (Text S2). Simulated backward particle trajectories were calculated from the day and location of deepest cesium observation (22 April 2013) to the day of the maximum FDNPP atmospheric deposition (15 March 2011). Although high resolution and data assimilating, HYCOM cannot be expected to reproduce the exact ocean state at any given time and location. To account for this inaccuracy, backward trajectories were released within a 1° × 1° region centered at the location of the deepest observed P02 2013 Cs_F (29.5 to 30.5°N and 165.56 to 166.56°E, henceforth referred to as the *release box*) and over the course of 2 weeks, that is, 7 days before and after the date of observation (15 April 2013 to 29 April 2013). Particles were released daily on a regular 150 × 150 grid inside the release box for a total of 315,000 trajectories over 14 days. A number of simulations with fewer trajectories were also run to determine that the number of particles used here was adequate (i.e., produced results statistically similar to runs with fewer trajectories). A forward trajectory simulation run from the region of maximum atmospheric deposition in 2011 out to 2013 was also conducted. See Text S3 for simulation setup details.

4. Results

4.1. Simulated Trajectories and Mixed Layer Depth

The backward trajectory paths were spread across a broad swath of the northwestern Pacific (Figure 3, light gray), suggesting a large range of possible pathways that could bring water parcels to the observed location via modeled oceanic currents on the $26.5\sigma_\theta$ isopycnal. FDNPP radionuclides were introduced at the surface in 2011; therefore, we focus on when and where the $26.5\sigma_\theta$ isopycnal interacted with (i.e., lay within) the mixed layer during that year, assuming that this is how Cs_F was introduced to this isopycnal. The mixed layer was estimated using the 0.03 kg m^{-3} difference criterion (de Boyer Montégut et al., 2004; Dong et al., 2008; Holte et al., 2017). All trajectories passing within ±3 days and ± 0.25° latitude and longitude of each interaction time/location were considered to have interacted with the mixed layer.

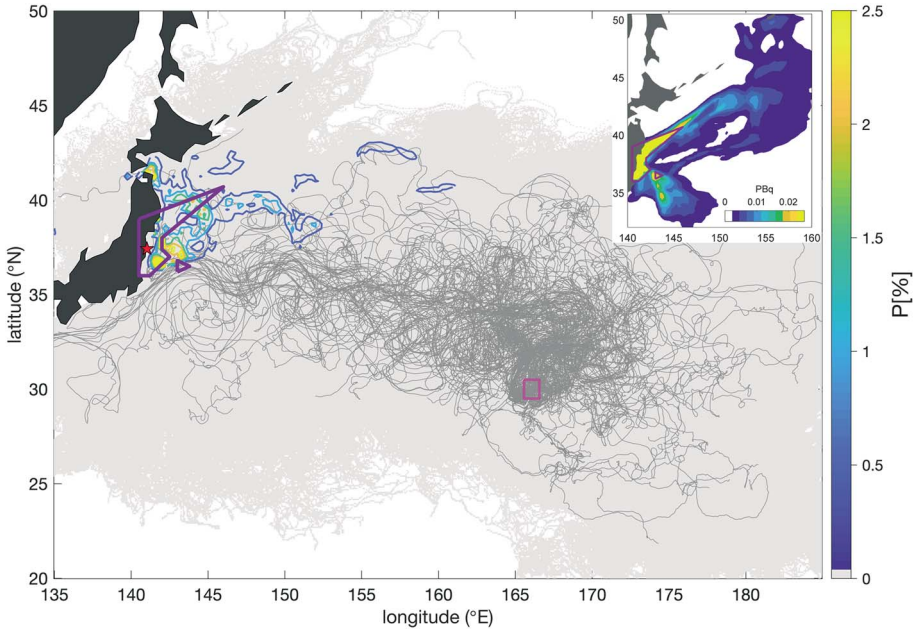

Figure 3. All particle backward trajectories (light gray) overlaid with random selection of trajectories (dark gray) as examples of trajectory behavior. Colored contours indicate the probability of a trajectory interacting with the mixed layer between 15 March 2011 and 31 December 2011. Highest probability is 4.5%, and color bar is saturated at 2.5%. The *release box* is outlined in pink. Red star indicates FDNPP location. Upper-right subplot is a model estimate of atmospheric deposition coverage and concentration adapted from Stohl et al. (2012); color scale blue (>0) to yellow (0.025 PBq). Purple polygon roughly outlines Stohl et al.'s estimate of concentration greater than 0.02 PBq (dark orange to yellow). FDNPP = Fukushima Daiichi Nuclear Power Plant.

Of the 24,954 trajectories that interacted with the mixed layer in 2011, the percentage of interactions in each 0.25° grid cell is shown in Figure 3 (color contours). The highest probabilities (≥2.5%) for mixed layer interaction can be seen in the immediate vicinity of the Japan coast, to the east of the FDNPP (yellow contours). These regions of mixed layer interaction overlap the Stohl et al. (2012) model-based estimate of the location of maximum atmospheric deposition (Figure 3 purple polygon and subpanel). This reassuring result confirms that the observed Cs_F likely originated from the vicinity of FDNPP in 2011. The model also suggests that the timing of the Fukushima accident (when mixed layers were deep and mode waters were being formed) was crucial to the $26.5\sigma_\theta$ isopycnal's exposure to radionuclides (Movie S1and Figure S3). During 2011, this exposure occurred within the purple polygon region most often between 19 and 26 March 2011 (Figure S4). Note that the purple polygon and the areas with the highest probability of mixed layer interaction overlap with the L-CMW, D-CMW, and TRMW formation regions (Figure 1), and the $26.5\sigma_\theta$ isopycnal lies within the density range of both the denser water masses, D-CMW and TRMW. Furthermore, the presence of high-interaction areas (Figure 3, yellow contours) within the polygon suggests that these denser water masses may have been forming as far south as ~36°N during the spring of 2011 (Figure S3, orange crosses). According to HYCOM, in the days following the March accident in 2011, the densest value attained by the mixed layer within the polygon ranged between 23.3 and $26.8\sigma_\theta$ but it was the denser waters in the range of 26.2–$26.6\sigma_\theta$ that were amongst the most common (Figure S5).

4.2. Probability and Arrival Date Maps

Of the 300,000+ particles released from the pink box (Figure 3), 6,772 (or 2.2%) trajectories interacted with the mixed layer inside the region of maximum atmospheric deposition (purple polygon in Figure 3) in 2011. Henceforth, these trajectories are referred to as *successful*. The statistical techniques of probability and arrival date mapping (Rypina, Jayne, et al., 2014; Rypina, Llopiz, et al., 2014; Rypina et al., 2016, 2019) were applied to the successful trajectories, to better understand the timing and pathways of the particles most likely to transport the Cs_F signal. Note, however, that even though trajectories were simulated backward

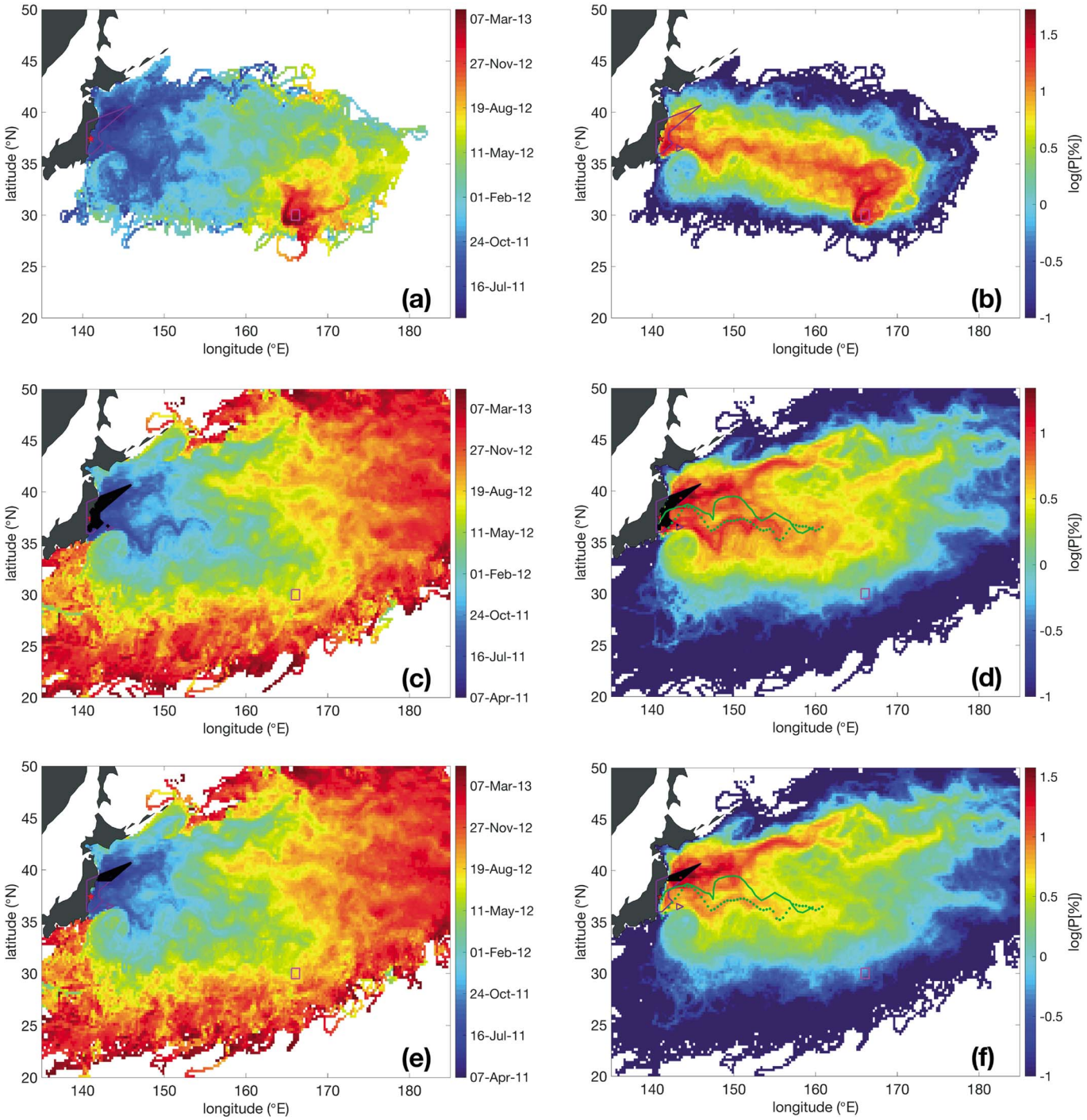

Figure 4. Maps representing the average arrival date at each 0.25° grid cell (a, c, e) and the percentage probability for trajectories to pass through each grid cell (b, d, f) for the different simulations: (a, b) successful backward trajectories, (c, d) forward trajectories, and (e, f) forward trajectories released north of 39°N. Green curves represent by way of example a single instance of the north wall of the KE (solid) based on a snapshot of sea surface height and temperature and an estimate of the climatological core of the current (dashed) based on hydrography (Isoguchi et al., 2006, interpretation of their Figures 3 and 2a, respectively). Symbols are the same as in Figure 3.

in time from the pink release box, we now discuss the movement of these fluid parcels forward in time from when they exited the purple polygon in 2011 to when they arrived in the release box.

The probability map (Figure 4b) represents the percentage of successful trajectories that visit different geographical locations throughout the study region. Probabilities were computed by gridding the domain into 0.25° × 0.25° bins, summing the number of successful trajectories that passed through each bin and dividing by the total number of successful trajectories. The 2-year timescale for the trip is illustrated in the arrival date map (Figure 4a), which shows the average first arrival of all successful trajectories to each bin.

The red colors in the probability map (Figure 4b) indicate the highest probability (~10% or more) and outline the most likely route for the water parcels associated with successful trajectories to travel from the purple polygon in 2011 to the observed location in 2013. This route runs eastward from Japan and extends along the path of the KE out into the western Pacific. The abrupt transition from red to yellow/green south of the KE between the coast and ~145°E indicates that on $26.5\sigma_\theta$ only a few successful trajectories crossed the KE within this longitudinal band to enter the recirculation region to the south, where NPSTMW is formed and where the subsurface Cs_F was found in 2012 in lighter waters (Aoyama et al., 2016; Kumamoto et al., 2014). Trajectories entering the recirculation region most likely crossed the KE to the east of 145°E and before recirculating anticyclonically. The arrival date map (Figure 4a) shows an associated abrupt transition from early arrival dates (dark blue) inside this fast-flowing segment of the KE as it first moves offshore to significantly later arrival dates (cyan/blue) just to the south. Both maps suggest limited entry to the recirculation region west of 145°E. Further east, the red/orange high-probability path widens and diffuses as the KE becomes less coherent. However, the highest probability path (brightest red) still lies along the track and to the north of the KE out to ~165–167°E, where the high-probability path turns sharply south, crossing the KE to arrive in the pink box. The probability that trajectories will cross the KE and head south toward the location of the 2013 observations is nearly 25% at 165°E, whereas near the recirculation, the probability is 1% or less (yellow/green colors). This result suggests that where the current is strongest, the KE is acting as a barrier to southward particle transport at the depth of the $26.5\sigma_\theta$ surface, at least for those trajectories that eventually arrive at the 30°N, 166°E observation location in 2013.

The forward trajectory simulation was used to investigate the fate of all water parcels on the $26.5\sigma_\theta$ surface (i.e., not just those that arrived in the pink box) that interacted with the mixed layer in the spring of 2011 inside the region of maximum atmospheric deposition (purple polygon) but did not necessarily end up at the observed *pink box* location. Separate maps were created for all forward trajectories (Figures 4c and 4d), and for forward trajectories beginning to the north (Figures 4e and 4f) and south (not shown) of 39°N. Results suggest that on $26.5\sigma_\theta$ there are two most probable pathways (reddest streaks, Figure 4c). One path heads to the northeast at 40°N as suggested by, for example, Rossi et al. (2013) and Aoyama et al. (2016). The second lies along the track of the KE. The barrier effect of the KE is less pronounced in the forward run, most likely because some particles released within the area of maximum atmospheric deposition appear to have been released on the *other side* of the KE, that is, east of Kuroshio from the southernmost portion of the purple polygon and south of KE from the small purple triangle (Figures 4f). These waters are free to spread southward without being bounded by the KE barrier. Supporting this hypothesis, when trajectories were initialized in the purple polygon to the north of the north wall of the Kuroshio (39°N in the spring of 2011), they largely remained to the north of the KE barrier out to 155–160°E (Figure 4f, KE highlighted by green curves based on Isoguchi et al., 2006), whereas trajectories that began to the south of this latitude were much more likely to be drawn into the recirculation near 145°E or to spread southward west of 160°E.

5. Conclusions

Output from a high-resolution numerical model is used to investigate possible pathways for $26.5\sigma_\theta$ waters (the densest 2013, 30°N waters with detectable Cs_F) from their formation regions in the MWR to where they were measured at depth south of the KE at 166°E. The 2011 FDNPP accidental discharge and the 2013 30°N observations set the timescale of the study. The subsurface distribution of Cs_F observed south of the KE has previously been explained in terms of subduction of mode water after formation, followed by mixing and advection (e.g., Aoyama et al., 2016; Kumamoto et al., 2014, 2017). We show that for $26.5\sigma_\theta$ waters, the denser variety of CMW, which have interacted with the mixed layer in the formation region, along-isopycnal advection is sufficient to explain the presence of C_{SF} at depths greater than 500 m south of the KE jet not only at 30°N, 166°E but also as far east as 179°E (Figures 2 and 4d). The most probable pathway for the deepest

observed 30°N Cs_F signal is along and to the north of the KE, with a southeastward turn just beyond 165°E. These waters, which begin their journey within the mixed layer (200–300 m), dive as they cross the front to where they were found at >500 m. Note that the observed cesium (Figure 2) does not represent the deepest signal but rather the depth of the deepest sampling location. Examination of the water densities reached by the deepest HYCOM model mixed layers in 2011 (Figure S5) suggests that had deeper samples been taken; this unique tracer might have been found in water as dense as $26.8\sigma_\theta$ at a depth of ~700 m.

While it has been shown that strong oceanic jets such as the Gulf Stream and the Kuroshio often act as (permeable) barriers to particle transport in surface waters (e.g., Rypina et al., 2011, 2013, 2018), the trajectory statistics calculated here suggest the same is true even at the depth of the $26.5\sigma_\theta$ density surface. The backward trajectory results indicate a well-defined major pathway following the northern edge of the KE from Japan to ~165°E (although this barrier is not absolute and some cross-frontal transport occurs west of 165°E), turning sharply south at this longitude. The forward trajectory run also suggests that $26.5\sigma_\theta$ waters that interacted with the mixed layer to the north of the north wall of the KE (39°N in 2011 HYCOM) are unlikely to cross the KE until they reach 155–160°E. It is only here that many of these trajectories cross and remain to the south of the front. However, because part of the atmospheric deposition (the southeastern part of our purple polygon and the small triangle) lies *on the southern side* of the KE, this signal is free to spread southward without being constrained by the KE barrier. The transport barrier near the KE core agrees with the strong Kolmogorov-Arnold-Moser stability arguments of Rypina et al. (2007, although these are not rigorously applicable to nonperiodic flows) and with more recent results by Farazmand et al. (2014) and Haller (2016) on parabolic transport barriers associated with shearless jet cores. It is also in line with the critical layer theory results of Ferrari and Nikurashin (2010) and Chen et al. (2014), who found limited subsurface cross-KE transport west of ~155°E, with enhanced meridional transport at this longitude.

Acknowledgments
We would like to thank our two anonymous reviewers for their insightful suggestions that improved this paper. Work by Cedarholm on this project was supported by the WHOI Summer Student Fellowship program and was her UNH senior Capstone project. Rypina, Macdonald, and Yoshida acknowledge salary and project support from the National Science Foundation (NSF) grant OCE-1356630. Additionally, Rypina would like to acknowledge support from NSF grant OCE-1558806. CLIVAR PO2 and P10 observations, data sets 318M20130321 and 49NZ2012011, were obtained from the CCHDO (https://cchdo.ucsd.edu/) and the HYCOM output, data set GLBa0.08 expt_90.0v, from https://www.hycom.org/. Argo profiles were obtained from http://www.argodatamgt.org, the ISAS-15 0.5°gridded Argo-data-alone product from https://www.seanoe.org, and delayed-time allsat AVISO gridded surface velocity estimates from http://marine.copernicus.eu. Extended acknowledgements in Text S4.

References

Aoyama, M., Hamajima, Y., Hult, M., Uematsu, M., Oka, E., Tsumune, D., & Kumamoto, Y. (2016). ^{134}Cs and ^{137}Cs in the North Pacific Ocean derived from the March 2011 TEPCO Fukushima Dai-ichi Nuclear Power Plant accident, Japan. Part one: surface pathway and vertical distributions. *Journal of Oceanography*, *72*(1), 53–65. https://doi.org/10.1007/s10872-015-0335-z

Argo. (2000). Argo float data and metadata from Global Data Assembly Centre (Argo GDAC). SEANOE. https://doi.org/10.17882/42182

Bingham, F. M., & Suga, T. (2006). Distributions of mixed layer properties in North Pacific water mass formation areas: Comparison of Argo floats and World Ocean Atlas 2001. *Ocean Science*, *2*(1), 61–70. https://doi.org/10.5194/os-2-61-2006

Bleck, R. (2002). An oceanic general circulation model framed in hybrid isopycnic-Cartesian coordinates. *Ocean Modelling*, *4*(1), 55–88. https://doi.org/10.1016/S1463-5003(01)00012-9

Bower, A. S., Rossby, H. T., & Lillibridge, J. L. (1985). The Gulf Stream—Barrier or blender? *Journal of Physical Oceanography*, *15*(1), 24–32. https://doi.org/10.1175/1520-0485(1985)015<0024:TGSOB>2.0.CO;2

Buesseler, K., Aoyama, M., & Fukasawa, M. (2011). Impacts of the Fukushima Nuclear Power Plants on marine radioactivity. *Environmental Science & Technology*, *45*(23), 9931–9935. https://doi.org/10.1021/es202816c

Buesseler, K., Dai, M., Aoyama, M., Benitez-Nelson, C., Charmasson, S., Higley, K., et al. (2017). Fukushima Daiichi-derived radionuclides in the ocean: Transport, fate, and impacts. *Annual Review of Marine Science*, *9*(1), 173–203. https://doi.org/10.1146/annurev-marine-010816-060733

Buesseler, K. O., Jayne, S. R., Fisher, N. S., Rypina, I. I., Baumann, H., Baumann, Z., et al. (2012). Fukushima-derived radionuclides in the ocean and biota off Japan. *Proceedings of the National Academy of Sciences of the United States of America*, *109*(16), 5984–5988. https://doi.org/10.1073/pnas.1120794109

Burkholder, K., & Lozier, M. (2011). Subtropical to subpolar pathways in the North Atlantic: Deductions from Lagrangian trajectories. *Journal of Geophysical Research*, *116*, C07017. https://doi.org/10.1029/2010JC006697

Burkholder, K. C., & Lozier, M. S. (2014). Tracing the pathways of the upper limb of the North Atlantic Meridional Overturning Circulation. *Geophysical Research Letters*, *41*, 4254–4260. https://doi.org/10.1002/2014GL060226

Chen, R., McClean, J. L., Gille, S. T., & Griesel, A. (2014). Isopycnal eddy diffusivities and critical layers in the Kuroshio Extension from an eddying ocean model. *Journal of Physical Oceanography*, *44*(8), 2191–2211. https://doi.org/10.1175/JPO-D-13-0258.1

Cummings, J. A., & Smedstad, O. M. (2013). Variational data assimilation for the global ocean. In S. K. Park & L. Xu (Eds.), *Data Assimilation for Atmospheric, Oceanic and Hydrologic Applications* (Vol. 2, pp. 303–343). Berlin, Heidelberg: Springer. https://doi.org/10.1007/978-3-642-35088-7_13

de Boyer Montégut, C., Madec, G., Fischer, A. S., Lazar, A., & Iudicone, D. (2004). Mixed layer depth over the global ocean: An examination of profile data and a profile-based climatology. *Journal of Geophysical Research*, *109*, C12003. https://doi.org/10.1029/2004JC002378

Dong, S., Sprintall, J., Gille, S. T., & Talley, L. (2008). Southern Ocean mixed-layer depth from Argo float profiles. *Journal of Geophysical Research*, *113*, C06013. https://doi.org/10.1029/2006JC004051

Farazmand, M., Blazevski, D., & Haller, G. (2014). Shearless transport barriers in unsteady two-dimensional flows and maps. *Physica D: Nonlinear Phenomena*, *278-279*, 44–57. https://doi.org/10.1016/j.physd.2014.03.008

Ferrari, R., & Nikurashin, M. (2010). Suppression of eddy diffusivity across jets in the Southern Ocean. *Journal of Physical Oceanography*, *40*(7), 1501–1519. https://doi.org/10.1175/2010JPO4278.1

Gaillard, F., Reynaud, T., Thierry, V., Kolodziejczyk, N., & von Schuckmann, K. (2016). In situ-based reanalysis of the global ocean temperature and salinity with ISAS: Variability of the heat content and steric height. *Journal of Climate*, *29*(4), 1305–1323. https://doi.org/10.1175/JCLI-D-15-0028.1

Garraffo, Z. D., Kim, H. C., Mehra, A., Spindler, T., Rivin, I., & Tolman, H. L. (2014). Modeling of ^{137}Cs as a tracer in a regional model for the western Pacific, after the Fukushima–Daiichi Nuclear Power Plant accident of March 2011. *Weather and Forecasting*, *31*(2), 553–579. https://doi.org/10.1175/WAF-D-13-00101.1

Gray, A. R., & Riser, S. C. (2014). A global analysis of sverdrup balance using absolute geostrophic velocities from Argo. *Journal of Physical Oceanography*, *44*(4), 1213–1229. https://doi.org/10.1175/JPO-D-12-0206.1

Haller, G. (2016). Dynamic rotation and stretch tensors from a dynamic polar decomposition. *Journal of the Mechanics and Physics of Solids*, *86*, 70–93. https://doi.org/10.1016/j.jmps.2015.10.002

Halliwell, G. R. (1998). Simulation of North Atlantic decadal/multidecadal winter SST anomalies driven by basin-scale atmospheric circulation anomalies. *Journal of Physical Oceanography*, *28*(1), 5–21. https://doi.org/10.1175/1520-0485(1998)028<0005:SONADM>2.0.CO;2

Holte, J., Talley, L. D., Gilson, J., & Roemmich, D. (2017). An Argo mixed layer climatology and database. *Geophysical Research Letters*, *44*, 5618–5626. https://doi.org/10.1002/2017GL073426

Isoguchi, O., Kawamura, H., & Oka, E. (2006). Quasi-stationary jets transporting surface warm waters across the transition zone between the subtropical and the subarctic gyres in the North Pacific. *Journal of Geophysical Research*, *111*, C10003. https://doi.org/10.1029/2005JC003402

Kolodziejczyk, N., Prigent-Mazella, A., & Fabienne, G. (2017). ISAS-15 temperature and salinity gridded fields. SEANOE. https://doi.org/10.17882/52367

Kumamoto, Y., Aoyama, M., Hamajima, Y., Aono, T., Kouketsu, S., Murata, A., & Kawano, T. (2014). Southward spreading of the Fukushima-derived radiocesium across the Kuroshio Extension in the North Pacific. *Scientific Reports*, *4*(1), 4276. https://doi.org/10.1038/srep04276

Kumamoto, Y., Aoyama, M., Hamajima, Y., Nagai, H., Yamagata, T., Kawai, Y., et al. (2017). Fukushima-derived radiocesium in the western North Pacific in 2014. *Journal of Radioanalytical and Nuclear Chemistry*, *311*(2), 1209–1217. https://doi.org/10.1007/s10967-016-5055-3

Millero, F. J., & Poisson, A. (1981). International one-atmosphere equation of state of seawater. *Deep Sea Research Part A. Oceanographic Research Papers*, *28*(6), 625–629. https://doi.org/10.1016/0198-0149(81)90122-9

Mizuno, K., & White, W. B. (1983). Annual and interannual variability in the Kuroshio current system. *Journal of Physical Oceanography*, *13*(10), 1847–1867. https://doi.org/10.1175/1520-0485(1983)013<1847:AAIVIT>2.0.CO;2

Rossi, V., van Sebille, E., Sen Gupta, A., Garçon, V., & England, M. H. (2013). Multi-decadal projections of surface and interior pathways of the Fukushima cesium-137 radioactive plume. *Deep Sea Research Part I: Oceanographic Research Papers*, *80*, 37–46. https://doi.org/10.1016/j.dsr.2013.05.015

Rypina, I. I., Brown, M. G., Beron-Vera, F. J., Koçak, H., Olascoaga, M. J., & Udovydchenkov, I. A. (2007). Robust transport barriers resulting from strong Kolmogorov-Arnold-Moser stability. *Physical Review Letters*, *98*(10), 104102. https://doi.org/10.1103/PhysRevLett.98.104102

Rypina, I. I., Chen, K., Hernández, C. M., Pratt, L. J., & Llopiz, J. K. (2019). Investigating the suitability of the slope sea for Atlantic bluefin tuna spawning using a high-resolution ocean circulation model. *ICES Journal of Marine Science*. https://doi.org/10.1093/icesjms/fsz079

Rypina, I. I., Fertitta, D., Macdonald, A., Yoshida, S., & Jayne, S. (2016). Multi-iteration approach to studying tracer spreading using drifter data. *Journal of Physical Oceanography*, *47*(2), 339–351. https://doi.org/10.1175/JPO-D-16-0165.1

Rypina, I. I., Jayne, S. R., Yoshida, S., Macdonald, A. M., & Buesseler, K. (2014). Drifter-based estimate of the 5 year dispersal of Fukushima-derived radionuclides. *Journal of Geophysical Research: Oceans*, *119*, 8177–8193. https://doi.org/10.1002/2014JC010306

Rypina, I. I., Jayne, S. R., Yoshida, S., Macdonald, A. M., Douglass, E. M., & Buesseler, K. O. (2013). Short-term dispersal of Fukushima-derived radionuclides off Japan: Modeling efforts and model-data intercomparison. *Biogeosciences*, *10*(7), 4973–4990. https://doi.org/10.5194/bg-10-4973-2013

Rypina, I. I., Llewellyn Smith, S. G., & Pratt, L. J. (2018). Connection between encounter volume and diffusivity in geophysical flows. *Nonlinear Processes in Geophysics*, *25*(2), 267–278. https://doi.org/10.5194/npg-25-267-2018

Rypina, I. I., Llopiz, J. K., Pratt, L. J., & Lozier, M. S. (2014). Dispersal pathways of American eel larvae from the Sargasso Sea. *Limnology and Oceanography*, *59*(5), 1704–1714. https://doi.org/10.4319/lo.2014.59.5.1704

Rypina, I. I., Pratt, L. J., & Lozier, M. S. (2011). Near-surface transport pathways in the north Atlantic Ocean: Looking for throughput from the subtropical to the subpolar gyre. *Journal of Physical Oceanography*, *41*(5), 911–925. https://doi.org/10.1175/2011JPO4498.1

Saito, H., Suga, T., Hanawa, K., & Shikama, N. (2011). The transition region mode water of the North Pacific and its rapid modification. *Journal of Physical Oceanography*, *41*(9), 1639–1658. https://doi.org/10.1175/2011JPO4346.1

Stohl, A., Seibert, P., Wotawa, G., Arnold, D., Burkhart, J. F., Eckhardt, S., et al. (2012). Xenon-133 and caesium-137 releases into the atmosphere from the Fukushima Dai-ichi nuclear power plant: Determination of the source term, atmospheric dispersion, and deposition. *Atmospheric Chemistry and Physics*, *12*(5), 2313–2343. https://doi.org/10.5194/acp-12-2313-2012

Talley, L. D., Nagata, Y., Fujimura, M., Iwao, T., Kono, T., Inagake, D., et al. (1995). North Pacific intermediate water in the Kuroshio/Oyashio mixed water region. *Journal of Physical Oceanography*, *25*(4), 475–501. https://doi.org/10.1175/1520-0485(1995)025<0475:NPIWIT>2.0.CO;2

Yoshida, S., Macdonald, A. M., Jayne, S. R., Rypina, I. I., & Buesseler, K. O. (2015). Observed eastward progression of the Fukushima 134Cs signal across the North Pacific. *Geophysical Research Letters*, *42*, 7139–7147. https://doi.org/10.1002/2015GL065259